5-24-2012

Flexure-FET biosensor to break the fundamental sensitivity limits of nanobiosensors using nonlinear electromechanical coupling

Ankit Jain
jankit@purdue.edu

Pradeep Nair
Purdue University

Muhammad A. Alam
Purdue University

Jain, Ankit; Nair, Pradeep; and Alam, Muhammad A., "Flexure-FET biosensor to break the fundamental sensitivity limits of nanobiosensors using nonlinear electromechanical coupling" (2012). *Birck and NCN Publications.* Paper 856.
http://dx.doi.org/10.1073/pnas.1203749109

Flexure-FET biosensor to break the fundamental sensitivity limits of nanobiosensors using nonlinear electromechanical coupling

Ankit Jain[1], Pradeep R. Nair, and Muhammad A. Alam[1]

School of Electrical and Computer Engineering, Purdue University, West Lafayette, IN 47907

Edited by L. B. Freund, University of Illinois, Urbana, IL, and approved March 30, 2012 (received for review March 5, 2012)

In this article, we propose a Flexure-FET (flexure sensitive field effect transistor) ultrasensitive biosensor that utilizes the nonlinear electromechanical coupling to overcome the *fundamental* sensitivity limits of classical electrical or mechanical nanoscale biosensors. The stiffness of the suspended gate of Flexure-FET changes with the capture of the target biomolecules, and the corresponding change in the gate shape or deflection is reflected in the drain current of FET. The Flexure-FET is configured to operate such that the gate is biased near pull-in instability, and the FET-channel is biased in the subthreshold regime. In this coupled nonlinear operating mode, the sensitivity (S) of Flexure-FET with respect to the captured molecule density (N_s) is shown to be *exponentially* higher than that of any other electrical or mechanical biosensor. In other words, while $S_{\text{Flexure}} \sim e^{(\gamma_1\sqrt{N_s}-\gamma_2 N_s)}$, classical electrical or mechanical biosensors are limited to $S_{\text{classical}} \sim \gamma_3 N_S$ or $\gamma_4 \ln(N_S)$, where γ_i are sensor-specific constants. In addition, the proposed sensor can detect both charged and charge-neutral biomolecules, without requiring a reference electrode or any sophisticated instrumentation, making it a potential candidate for various low-cost, point-of-care applications.

label-free detection | genome sequencing | cantilever | spring-softening | critical-point sensors

Nanoscale biosensors are widely regarded as a potential candidate for ultrasensitive, label-free detection of biochemical molecules. Among the various technologies, significant research have focused on developing ultrasensitive nanoscale electrical (1) and mechanical (2) biosensors. Despite remarkable progress over the last decade, these technologies have fundamental challenges that limit opportunities for further improvement in their sensitivity (Fig. 1*A*) (3–6). For example, the sensitivity of electrical nanobiosensors such as Si-Nanowire (NW) FET (field effect transistor) (Fig. 1*B*) is severely suppressed by the electrostatic screening due to the presence of other ions/charged biomolecules in the solution (7), which limits its sensitivity to vary *linearly* (in subthreshold regime) (3, 7) or *logarithmically* (in accumulation regime) (4, 7, 8, 9) with respect to the captured molecule density N_s. Moreover, the miniaturization and stability of the reference electrode have been a persistent problem, especially for lab-on-chip applications (1). Finally, it is difficult to detect charge-neutral biological entities such as viruses or proteins using charge-based electrical nanobiosensor schemes.

In contrast, nanomechanical biosensors like nanocantilevers (10, 11) (Fig. 1*C*) do not require biomolecules to be charged for detection. Here, the capture of target molecules on the cantilever surface modulates its mass, stiffness, and/or surface stress (5, 11, 12). This change in the mechanical properties of the cantilever can then be observed as a change in its resonance frequency (dynamic mode), mechanical deflection, or change in the resistance of a piezoresistive material (static mode) attached to the cantilever (6, 13). Unfortunately, typical optical detection schemes (10) require complex instrumentation which may preclude them from many low-cost point-of-care applications. Further, the response of nanomechanical biosensors varies only linearly (5) or logarithmically (6, 14, 15) with the change in the mass or surface stress of the cantilever, and therefore these sensors may not be sufficiently sensitive to detect target molecules at very low analyte concentrations, unless sophisticated, low-noise setup is used.

To overcome the respective limitations of classical electrical and mechanical nanoscale biosensors, we propose the concept of a Flexure-FET biosensor that integrates the key advantages of both technologies but does not suffer from the limitations of either approach. The Flexure-FET consists of a nanoplate channel biased through a thin-film suspended gate (Fig. 1*D*). Although the structure is similar to that of a suspended-gate FET (16), nano-electromechanical (NEM) FET (17), or resonant gate transistor (18), we call the device Flexure-FET to emphasize its distinctive nonlinear operation specifically optimized for ultrasensitive detection of biomolecules. As shown in Fig. 1*E*, the ultra high sensitivity arises from the coupling of two electromechanical nonlinear responses, namely (*i*) spring-softening (19) in which stiffness decreases nonlinearly with the applied gate bias V_G and vanishes at the pull-in point (for detailed discussions on pull-in instability, see refs. 20, 21), and (*ii*) subthreshold electrical conduction (22) in which current depends exponentially on the surface potential (Fig. S1). Such nonlinear electromechanical coupling enables exponentially high sensitivity for Flexure-FET sensors (Fig. 1*A*), which is fundamentally unachievable by exclusive use of existing nanoscale electrical or mechanical biosensors. Moreover, the reliance of change in stiffness (23, 24) ensures screening-free detection of charged/neutral molecules, with no need for a reference electrode, and the measurement of drain current for detection requires no complex instrumentation. It should be noted that from a mechanical perspective, the Flexure-FET operates close to pull-in instability, a critical point. Similar critical point sensing has also been reported for vapor sensors (25) that operate close to bucking-instability (25) and for mass sensors that operate close to saddle-node bifurcation (26), and their higher sensitivity has been confirmed experimentally. However, beyond the critical point sensing, the integrated transistor-action in the subthreshold regime provides the Flexure-FET an additional exponential sensitivity (and simpler direct current readout) that could not be achieved by the classical nonlinear sensor schemes.

Theory of Flexure-FET

Sensor Configuration Before Target Capture. The operating principle of Flexure-FET can be understood using the well established

Author contributions: A.J., P.R.N., and M.A.A. designed research; A.J. performed research; A.J., P.R.N., and M.A.A. analyzed data; and A.J., P.R.N., and M.A.A. wrote the paper.

The authors declare no conflict of interest.

This article is a PNAS Direct Submission.

[1]To whom correspondence may be addressed. E-mail: jankit@purdue.edu or alam@purdue.edu.

This article contains supporting information online at www.pnas.org/lookup/suppl/doi:10.1073/pnas.1203749109/-/DCSupplemental.

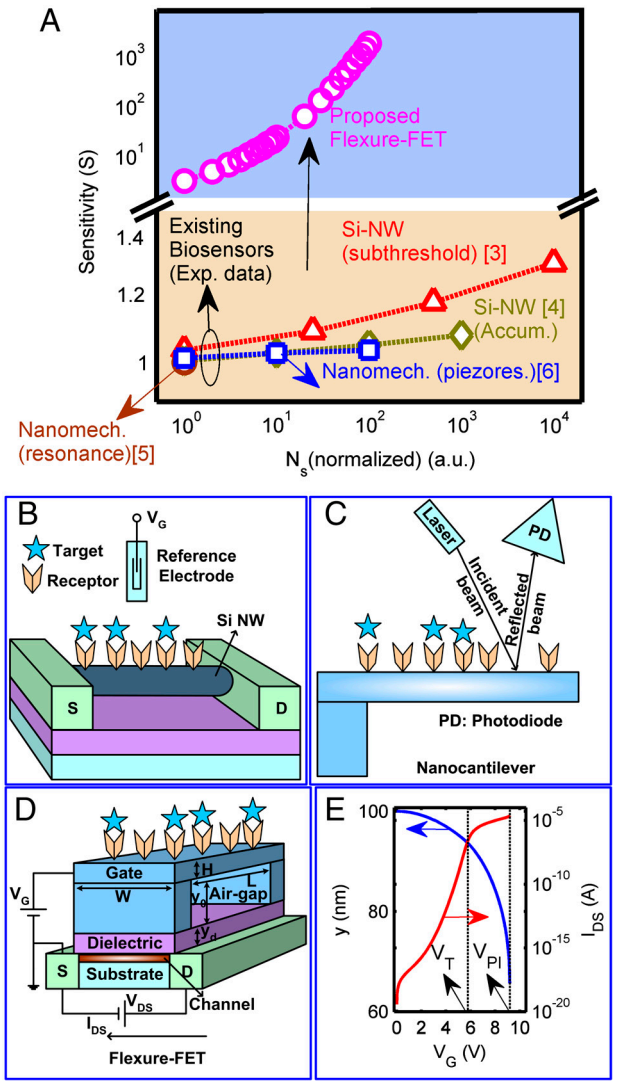

Fig. 1. (*A*) Sensitivity *S* of different types of biosensors; e.g., (*B*) electrical (Si-NW FET) in which transduction is achieved by modulation of channel conductivity (*G*) when charged biomolecules are captured by the gate. (*C*) Transduction in cantilever-based nanomechanical biosensors is achieved by change in its mass, stiffness, or surface stress. Nanocantilever can be operated in dynamic mode (mass change-based detection using shift in resonance frequency) or in static mode (surface stress change based detection using piezoresistive material). (*D*) Proposed Flexure-FET biosensor in which transduction is achieved due to change in the stiffness of the suspended gate. (*E*) Operation of Flexure-FET below pull-in. Displacement of the suspended gate (y) and drain current (I_{DS}) as a function of applied gate bias V_G. The y changes rapidly near pull-in ($V_G \approx V_{PI}$) and I_{DS} increases exponentially with V_G in the subthreshold regime ($V_G < V_T$).

spring-mass model (Fig. 2) (17, 18). With the application of gate bias V_G, the gate moves downward toward the dielectric (y vs. V_G curve in Fig. 1*E*), and the corresponding increase in gate capacitance is reflected in the increased drain current I_{DS}, as shown in Fig. 1*E*. The static behavior of the device is dictated by the balance of spring and electrostatic forces; i.e.,

$$k(y_0 - y) = \frac{1}{2}\epsilon_0 E_{air}^2 A, \qquad [1]$$

where $k = \frac{\alpha E W H^3}{12 L^3}$ is the stiffness, α is a geometrical factor, E is the Young's modulus, W is the width, H is the thickness, L is the length of the gate electrode, y_0 is the air-gap, y is the position of the gate electrode, ϵ_0 is the permittivity of free space, E_{air} is the electric field in the air, and $A = WL$ is the area of the gate

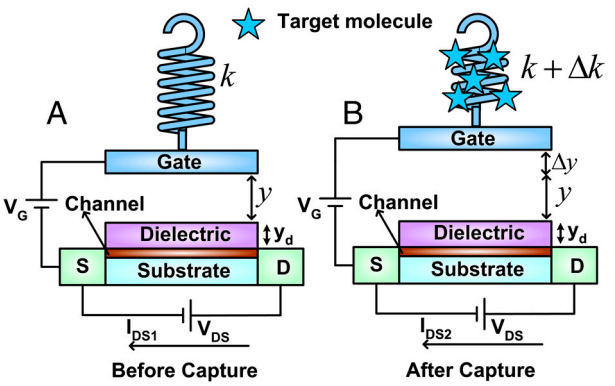

Fig. 2. (*A*) and (*B*). Equivalent spring-mass model of Flexure-FET. Stiffness changes from k to $k + \Delta k$ after the capture of biomolecules, and therefore position of the gate changes from y to $y + \Delta y$, which results in the modulation of drain current from I_{DS1} to I_{DS2}.

electrode. The electric field below the membrane E_{air} is equal to $\epsilon_s E_s(\psi_s)$, where ϵ_s is the dielectric constant of the substrate, and

$$E_s(\psi_s) = \sqrt{\frac{2qN_A}{\epsilon_0\epsilon_s}}\left[\psi_s + \left(e^{-\frac{q\psi_s}{k_B T}} - 1\right)\frac{k_B T}{q} - \left(\frac{n_i}{N_A}\right)^2\left(\psi_s - \left(e^{\frac{q\psi_s}{k_B T}} - 1\right)\frac{k_B T}{q}\right)\right]^{\frac{1}{2}}, \qquad [2a]$$

where $E_s(\psi_s)$ is the electric field at the substrate-dielectric interface (22, page 64, for a detailed derivation of Eq. **2a**), ψ_s is the surface potential, q is the charge of an electron, N_A is the substrate doping, k_B is the Boltzmann constant, T is the absolute temperature, and n_i is the intrinsic carrier concentration in the substrate. The voltage drop in air ($y\epsilon_s E_s(\psi_s)$), dielectric ($\frac{y_d}{\epsilon_d}\epsilon_s E_s(\psi_s)$), and substrate ($\psi_s$) can be related to the applied gate bias V_G as follows-

$$V_G = \left(y + \frac{y_d}{\epsilon_d}\right)\epsilon_s E_s(\psi_s) + \psi_s, \qquad [2b]$$

where, y_d is the dielectric thickness and ϵ_d is the dielectric constant. Eqs. **1** and **2** are solved self-consistently for y and ψ_s at each V_G. The corresponding inversion charge density (Q_i) in the channel and drain current (I_{DS}) are given by

$$Q_i = \frac{qn_i^2}{N_A}\int_0^{\psi_s} \frac{e^{\frac{q\psi}{k_B T}} - 1}{E_s(\psi)}\, d\psi, \qquad [3]$$

$$I_{DS} = \mu_n L Q_i \frac{V_{DS}}{W}, \qquad [4]$$

where μ_n is the channel mobility for electrons, V_{DS} is the applied drain to source voltage. Fig. 1*E* shows the steady-state response of Flexure-FET as a function of biasing voltage V_G, obtained from the numerical simulations of Eqs. **1**–**4**.

Flexure-FET Response to Target Capture. For transduction, the proposed Flexure-FET biosensor utilizes the change in suspended gate stiffness from k to $k + \Delta k$, (12, 24, 27–29) due to the capture of biomolecules. The change in stiffness due to the capture of biomolecules has been demonstrated by several recent experiments of mass sensing using nanocantilever-based resonators (12, 27, 28) (Fig. S2). This well known observation of stiffness change has been attributed to the change in the membrane thickness, Young's modulus, and/or surface stress of the beam (12, 23,

24, 30). Indeed, Craighead (27) suggests its use as a basis of a new class of mechanical biosensor.

In the following analysis, we model change in k by change in the effective thickness H of the gate (ΔH), although it should be stressed that the conclusions do not depend on the particular hypothesis regarding Δk. For now, we ignore the details of the spatial distribution of molecules associated with random sequential adsorption (31) and assume a uniform distribution of adsorbed molecules on the sensor surface. Therefore, the conservation of volume suggests $\Delta H = N_s A_t H_t$, where N_s is the area density, A_t is the effective cross-sectional area, and H_t is the effective thickness of the target molecule. Using the fact that $k = \frac{\alpha E W H^3}{12 L^3}$, the change in stiffness Δk due to $\Delta H (\ll H)$ can be related to adsorbed molecule density N_s as follows:

$$\frac{\Delta k}{k} \approx \frac{3 N_s A_t H_t}{H}. \qquad [5]$$

For simplicity, we have taken the Young's modulus of captured molecules to be the same as that of the membrane, but this is obviously not necessary, and the theory can be generalized by the methods developed in Tamayo, Ramos, Mertens, and Calleja (23).

Combining Eqs. **1** and **2b**, we get $k(y_0 - y)y^2 \approx \epsilon_0 A (V_G - \psi_s)^2/2$. Now, the change in gate position Δy for small change in stiffness Δk due to capture of biomolecules is given as

$$(3y - y_0)\Delta y^2 + y(3y - 2y_0)\Delta y \approx \frac{\epsilon_0 A (V_G - \psi_s)^2}{2}\frac{\Delta k}{k^2}. \qquad [6]$$

If Flexure-FET is biased close to pull-in ($V_G \approx V_{PI}, y \approx \frac{2}{3} y_0$), the nonlinear Δy^2 term dominates the linear Δy term in Eq. **6**. It is essential to bias the Flexure-FET in this nonlinear, close-to-pull-in regime for maximum sensitivity. Using Eqs. **5** and **6**, we find

$$\Delta y \approx \sqrt{\frac{\epsilon_0 A (V_G - \psi_s)^2}{2(3y - y_0)}\frac{\Delta k}{k^2}} \approx \beta \sqrt{N_s}, \qquad [7]$$

where $\beta = \sqrt{\frac{3\epsilon_0 A (V_G - \psi_s)^2}{2(3y - y_0)}\frac{A_t H_t}{H k}}$ is a bias and device dependent constant.

Since the electrostatic force in subthreshold regime is given by $\frac{1}{2}\epsilon_0 E_{air}^2 A = q\epsilon_s \psi_s N_A A$ (Eq. **2a**), the corresponding change in the surface potential $\Delta\psi_s$ is obtained by perturbation of Eq. **1**; i.e.,

$$\Delta\psi_s \approx \frac{-k\Delta y + \Delta k(y_0 - y)}{q\epsilon_s N_A A}. \qquad [8]$$

Using Eqs. **2a**, **3**, and **4**, we can calculate the drain current I_{DS} in the subthreshold regime as follows,

$$I_{DS} \approx \frac{\mu_n L \left(\frac{V_{DS}}{W}\right)\left(\frac{q n_i^2}{N_A}\right)\left(\frac{k_B T}{q}\right) e^{\frac{q\psi_s}{k_B T}}}{\sqrt{\frac{2qN_A}{\epsilon_0 \epsilon_s}}\sqrt{\psi_s}}. \qquad [9]$$

Now, the ratio of the drain current before (I_{DS1}) and after (I_{DS2}) capture of biomolecules (in terms of the change in surface potential $\Delta\psi_s$) is given by

$$\frac{I_{DS1}}{I_{DS2}} \approx \exp\left(-\frac{q\Delta\psi_s}{k_B T}\right). \qquad [10]$$

Using Eqs. **8** and **10**, the ratio I_{DS1}/I_{DS2} is given by

$$\frac{I_{DS1}}{I_{DS2}} \approx \exp\left(\frac{k\Delta y - \Delta k(y_0 - y)}{k_B T \epsilon_s N_A A}\right). \qquad [11]$$

Therefore, if Flexure-FET is operated close to pull-in and in subthreshold regime, sensitivity S (using Eqs. **5**, **7**, and **11**) is given by

$$S_{Flexure} \equiv \frac{I_{DS1}}{I_{DS2}} \approx \exp(\gamma_1 \sqrt{N_s} - \gamma_2 N_s), \qquad [12]$$

where $\gamma_1 = \frac{k\beta}{k_B T \epsilon_s N_A A}$ and $\gamma_2 = \frac{3(y_0 - y)k A_t H_t}{k_B T \epsilon_s N_A A H}$. The sensitivity S is defined as I_{DS1}/I_{DS2}, because I_{DS} decreases after capture (see next text section).

Eq. **12** is the key result of the paper and shows how nonlinear interaction between mechanical (spring-softening) and electrical (subthreshold) aspects of sensing leads to an exponential sensitivity to capture of biomolecules. Such gain in sensitivity is impossible to achieve exclusively by electrical or mechanical sensing mechanisms.

Numerical Confirmation of Flexure-FET Response. The compact analytical expression of sensitivity of the Flexure-FET sensor can be validated by the self-consistent numerical solution of Eqs. **1**–**4**. The results for the change in sensor characteristics due to the capture of biomolecules are summarized in Fig. 3. For example, Fig. 3*A* shows y vs. V_G before and after capture of target molecules. After the capture, the gate moves up (for a fixed V_G) due to increased restoring spring force (because of increase in the k; Fig. 3*A*). Interestingly, change in gate position Δy is maximum close to pull-in due to spring-softening effect, as shown in Fig. 3*B* (see Figs. S3, S4 and S5 in *SI Text* for experimental validation). The change in gate position Δy is directly reflected in change in I_{DS}. Fig. 3*C* shows I_{DS} vs. V_G before and after capture of biomolecules. Interestingly, I_{DS} decreases after capture due to increased separation between the gate and the dielectric (hence decreased capacitance). The corresponding ratio of the currents

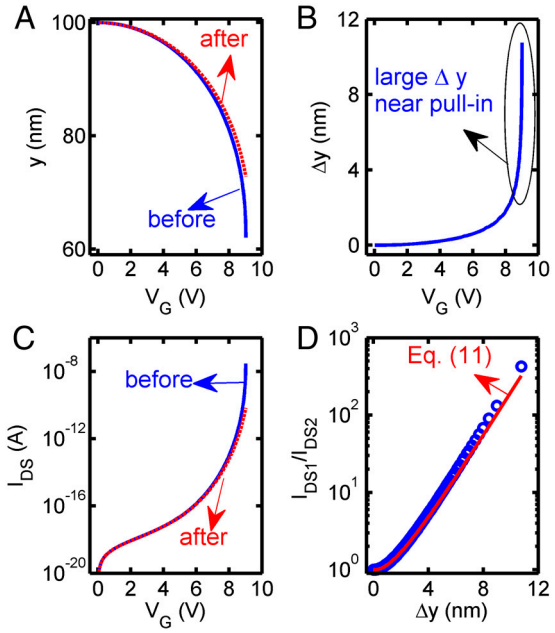

Fig. 3. Change in the sensor characteristics due to capture of target molecules on the surface of the gate, (*A*) y vs. V_G before and after capture, and (*B*) corresponding change in the position of gate electrode Δy vs. V_G. The Δy increases rapidly near pull-in due to spring-softening effect. The capture of target molecules is directly mirrored in the change in I_{DS}. (*C*) I_{DS} vs. V_G before and after capture, and (*D*) corresponding ratio of the two currents I_{DS1} (before capture) and I_{DS2} (after capture) as a function of Δy. Symbols denote the numerical simulation and solid line analytical formula (Eq. **11**). The device considered has the following typical parameters: $L = 4$ μm, $W = 1$ μm, $H = 40$ nm, $E = 200$ GPa, $y_0 = 100$ nm, $y_d = 5$ nm, $\epsilon_s = 11.7$, $\epsilon_d = 3.9$, $N_A = 6e16$ cm^{-3}.

I_{DS1} (before capture) and I_{DS2} (after capture) increases exponentially with Δy (Fig. 3*D*), and becomes maximum near pull-in. Note that the results from detailed numerical simulations are accurately anticipated by Eq. **11**, thus validating the analytical model described in the previous section. Therefore, by operating the Flexure-FET close to mechanical pull-in and in electrical subthreshold regime, orders of magnitude change in I_{DS} can be easily achieved for typical surface density of $N_s = 5 \times 10^{12}$ cm^{-2}, projected area of the biomolecule, $A_t = \pi R_t^2$ with $R_t = 1$ nm, and $H_t = 5.1$ nm. These parameters translate to just an equivalent $\Delta k \sim 6\%$. Note that to achieve the maximum sensitivity, it is important to bias the Flexure-FET in subthreshold regime below pull-in (i.e., $V_T \approx V_{PI}$).

Comparison with Classical Sensors

Next we compare the sensitivity of the proposed Flexure-FET sensor with the current nanoscale electrical/mechanical biosensors. Fig. 4*A* indicates that the Flexure-FET sensors are exponentially sensitive to change in stiffness or captured molecule density N_s (symbols: numerical simulation, solid line: analytical result; Eq. **12**). In the following, we explain the origin of linear (or logarithmic) sensitivity for electrical and mechanical nanoscale biosensors.

Electrical Nanobiosensors. For Si-NW FET biosensors, which also have the optimal sensitivity in subthreshold regime (3), sensitivity S is defined to be the ratio of conductance G (after) and G_0 (before) capture of target molecules (assuming conductance increases after the capture). Therefore, using Eq. **9**, S can be approximated as

$$S_{\mathrm{SiNW}} \equiv \frac{G}{G_0} \approx \exp\left(\frac{q\Delta\psi_s}{k_B T}\right). \qquad [13]$$

Unfortunately, the detection of biomolecules in a fluidic environment involves electrostatic screening by other ions in the solution.

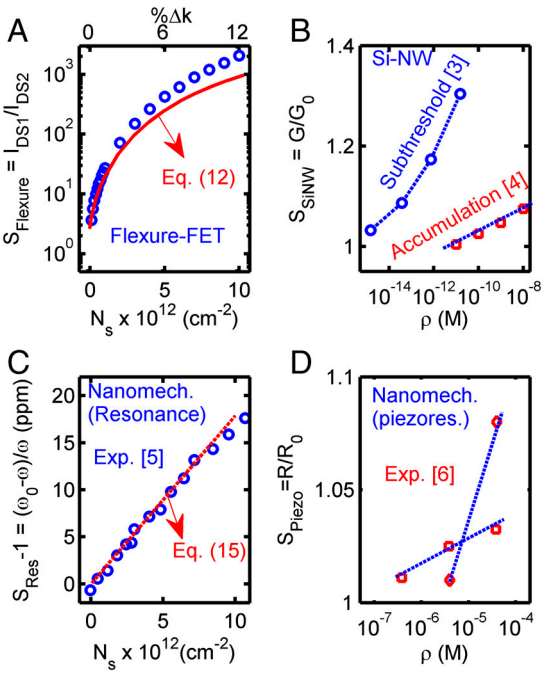

Fig. 4. Comparison of the sensitivity of different biosensors. Sensitivity S (*A*) Flexure-FET (symbols denote the numerical simulation). (*B*) Si-NW biosensors in subthreshold and accumulation regime. (*C*) Resonance mode nanomechanical biosensors. (*D*) Surface stress change-based piezoresistive nanomechanical biosensors, as a function of N_s or ρ. In (*B–D*), symbols are the experimental data and the line is the guide to the eye.

Consequently, the surface potential scales logarithmically with biomolecule density; i.e., $(q/k_B T)\Delta\psi_s \propto \ln(\delta N_s)$ (7) , where δ is a constant that depends on ionic strength and properties of dielectric/fluid interface. Therefore, optimal sensitivity of Si-NW biosensors is given by

$$S_{\mathrm{SiNW}} \propto \delta N_s. \qquad [14]$$

In Fig. 4*B*, S is plotted against volume concentration ρ, as the captured molecule density $N_s \propto \rho$ [linear regime of Langmuir isotherm (7)]. Therefore, all the conclusions regarding the dependence of sensitivity on N_s also hold for ρ. It should be noted that the reported sensitivity in the subthreshold regime (3) is actually sublinear (Fig. 4*B*), below the maximum sensitivity limit defined by Eq. **14** that can be achieved in this sensing regime. In the accumulation or the inversion regimes, $S_{\mathrm{SiNW}} \propto \Delta\psi_s$ (7), and therefore, $S_{\mathrm{SiNW}} \propto \ln(N_s)$, as shown in Fig. 4*B* (4, 7). Similar logarithmic dependence of sensitivity was reported in other references (8, 9) as well.

Mechanical Nanobiosensors. For nanomechanical biosensors such as resonance mode nanocantilever, the sensitivity S is defined as ω_0/ω, where ω is the resonance frequency after the capture of target biomolecules, and ω_0 is the resonance frequency before capture. Using the well known fact that $\omega = \sqrt{\frac{k}{m}}$, where k is the stiffness and m is the initial mass of the cantilever, S is given by

$$S_{\mathrm{Res}} \equiv \frac{\omega_0}{\omega} \approx 1 + \frac{1}{2}\frac{\Delta m}{m} = 1 + \frac{1}{2}\frac{N_s W L m^*}{m}, \qquad [15]$$

where m^* is the mass of individual biomolecule and $\Delta m = N_s W L m^*$ is the added mass of the biomolecules. Therefore, the sensitivity of mechanical biosensor can only vary linearly with N_s. This theoretical prediction is confirmed by experimental data (5) in Fig. 4*C*. We emphasize that the nanomechanical biosensors—with careful design and appropriate instrumentation—can be extraordinarily sensitive; indeed, zeptogram mass detection (32) has been reported. Eq. **15** simply suggests that the sensitivity of such sensor still varies linearly with respect to N_s.

It is also important to realize that the linear sensitivity with N_s is achieved only if the change in stiffness due to capture of molecules is negligible. In general, however, capture of target molecules increases stiffness of the membrane. If this increase in stiffness compensates the corresponding increase in the mass, there might be no change in resonance frequency at all (12, 28), and the sensitivity could be vanishingly small. One must independently measure the change in the stiffness (29, 30) to decouple the mass effect from stiffness effect so that the mass of the adsorbed molecule can be correctly estimated. In contrast, the Flexure-FET relies only on the change in the stiffness and works in the static mode, and therefore requires no more than a simple measurement of the drain current.

Another class of nanocantilever sensor involves operation in the static mode, where the capture of the target molecules introduces a surface stress, which in turn bends the cantilever. The displacement Δy of the tip can in principle be measured using sophisticated optical readout methods, but a simpler approach can be used instead: One can measure the change in surface stress by measuring the change in the resistance of a piezoresistor attached to the cantilever. For these piezoresistive-based cantilever biosensors, the sensitivity is defined as the ratio of resistance before (R_0) and after (R) the capture of biomolecules. Fig. 4*D* shows a logarithmic dependence of S on ρ. Similar logarithmic dependence for surface stress change has also been reported (14, 15). We therefore conclude that these static mode sensors do not exceed linear sensitivity limit of classical sensors.

We summarize the results discussed in this section in Fig. 1*A*, where the sensitivity of various types of nanobiosensors has been plotted against normalized N_s, *defined* as the ratio of the measured quantity (either ρ or N_s) to the minimum measured ρ or N_s of the available data. Fig. 1*A* allows us to conclude that the Flexure-FET biosensor will be exponentially more sensitive compared to existing nanoscale electrical or mechanical biosensors.

Finally, we emphasize that each of the three sequential physical phenomena associated with the operation of Flexure-FET (stiffness change due to capture of biomolecules, pull-in instability, subthreshold conduction) (Fig. S1) has been individually confirmed by numerous experiments based on electromechanical resonators (18, 33) and suspended-gate FET (34). We provide a summary of these experiments in the *SI Text* (Figs. S2, S4, S5, and S6). In the *SI Text*, we also suggest that a simple reconfiguration of existing electromechanical resonators or suspended-gate FET in Flexure-FET mode can give rise to exponential sensitivity (Fig. S7).

Conclusion

In this paper, we have demonstrated how the Flexure-FET nanobiosensor achieves exponentially high sensitivity by combining two nonlinear characteristics of spring-softening and subthreshold conduction. This extreme high sensitivity of Flexure-FET, therefore, breaks the fundamental limits of linear or logarithmic sensitivity of classical nanoscale electrical or mechanical biosensors. There are broad ranges of applications that can benefit from this sensitivity gain. For example, the current genome sequencing schemes require PCR (polymerase chain reaction) amplification of DNA strands because of the lower sensitivity of existing biosensors. The high sensitivity of Flexure-FET can eliminate the requirement of multiplication step and hence reduce the cost of sequencing. In addition, we recall that the proposed sensing scheme (*i*) can detect both charged and charge-neutral molecules, (*ii*) does not rely on reference electrode (the fundamental roadblock of Si-NW type biosensors), and (*iii*) obviates the need for any sophisticated and difficult-to-integrate instrumentation. The sensitivity of Flexure-FET can be further enhanced by choosing a softer membrane (having low stiffness) such as some polymer with low Young's modulus or an ultrathin membrane like graphene. Finally, let us emphasize that the sensing scheme is very general, which converts any change in the mechanical property of the gate electrode or change in the air-gap to the change in the drain current of the FET channel. Therefore, the proposed idea is not necessarily restricted to biomolecules detection but should find broader applications in gas/chemical/pressure sensing as well.

ACKNOWLEDGMENTS. We acknowledge discussions with Prof. R. Bashir (University of Illinois at Urbana-Champaign) and Jonghyun Go, financial support from National Institutes of Health (NIH, R01-CA20003), Materials, Structures and Devices (MSD) Focus Center, PRISM center, and computational resources from Network for Computational Nanotechnology (NCN).

1. Bergveld P (2003) Thirty years of ISFETOLOGY—What happened in the past 30 years and what may happen in the next 30 years. *Sensor Actuat B-Chem* 88(1):1–20.
2. Arlett J, Myers E, Roukes M (2011) Comparative advantages of mechanical biosensors. *Nat Nanotechnol* 6:203–215.
3. Gao X, Zheng G, Lieber C (2010) Subthreshold regime has the optimal sensitivity for nanowire FET biosensors. *Nano Lett* 10:547–552.
4. Bunimovich Y, et al. (2006) Quantitative real-time measurements of DNA hybridization with alkylated nonoxidized silicon nanowires in electrolyte solution. *J Am Chem Soc* 128:16323–16331.
5. Ekinci K, Roukes M (2005) Nanoelectromechanical systems. *Rev Sci Instrum* 76 (061101):1–12.
6. Wee K, et al. (2005) Novel electrical detection of label-free disease marker proteins using piezoresistive self-sensing micro-cantilevers. *Biosens Bioelectron* 20:1932–1938.
7. Nair P, Alam M (2008) Screening-limited response of nanobiosensors. *Nano Lett* 8:1281–1285.
8. Cheng M, et al. (2006) Nanotechnologies for biomolecular detection and medical diagnostics. *Curr Opin Chem Biol* 10:11–19.
9. Zheng G, Patolsky F, Cui Y, Wang W, Lieber C (2005) Multiplexed electrical detection of cancer markers with nanowire sensor arrays. *Nat Biotechnol* 23:1294–1301.
10. Lavrik N, Sepaniak M, Datskos P (2004) Cantilever transducers as a platform for chemical and biological sensors. *Rev Sci Instrum* 75:2229–2253.
11. Hwang K, Lee S, Kim S, Lee J, Kim T (2009) Micro- and nanocantilever devices and systems for biomolecule detection. *Annu Rev Anal Chem* 2:77–98.
12. Gupta A, et al. (2006) Anomalous resonance in a nanomechanical biosensor. *Proc Natl Acad Sci USA* 103:13362–13367.
13. Boisen A, Thundat T (2009) Design & fabrication of cantilever array biosensors. *Mater Today* 12:32–38.
14. Wu G, et al. (2001) Bioassay of prostate-specific antigen (PSA) using microcantilevers. *Nat Biotechnol* 19:856–860.
15. Zhang J, et al. (2006) Rapid and label-free nanomechanical detection of biomarker transcripts in human RNA. *Nat Nanotechnol* 1:214–220.
16. Abele N, et al. (2005) Suspended-Gate MOSFET: bringing new MEMS functionality into solid-state MOS transistor. *Proceedings of IEEE International Electron Device Meeting (IEDM)* pp 479–481.
17. Kam H, Lee DT, Howe RT, King T-J (2005) A new nano-electro-mechanical field effect transistor (NEMFET) design for low-power electronics. *Proceedings of IEEE International Electron Device Meeting (IEDM)* pp 463–466.
18. Nathanson HC, Newell WE, Wickstrom RA, Davis JR, Jr (1967) Resonant gate transistor. *IEEE Trans Electron Dev* 14:117–133.
19. Torun H, Sarangapani K, Degertekin F (2007) Spring constant tuning of active atomic force microscope probes using electrostatic spring softening effect. *Appl Phys Lett* 91(253113):1–3.
20. Krylov S, Maimon R (2004) Pull-in dynamics of an elastic beam actuated by continuously distributed electrostatic force. *J Vib Acoust* 126:332–342.
21. Krylov S (2007) Lyapunov exponents as a criterion for the dynamic pull-in instability of electrostatically actuated microstructures. *Int J NonLinear Mech* 42:626–642.
22. Yuan T, H NT (1998) *Fundamentals of Modern VLSI Devices* (Cambridge Univ Press, Cambridge, United Kingdom).
23. Tamayo J, Ramos D, Mertens J, Calleja M (2006) Effect of the adsorbate stiffness on the resonance response of microcantilever sensors. *Appl Phys Lett* 89(224104):1–3.
24. Waggoner P, Craighead H (2009) The relationship between material properties, device design, and the sensitivity of resonant mechanical sensors. *J Appl Phys* 105 (054306):1–14.
25. Southworth D, Bellan L, Linzon Y, Craighead H, Parpia J (2010) Stress-based vapor sensing using resonant microbridges. *Appl Phys Lett* 96(163503):1–3.
26. Kumar V, et al. (2011) Bifurcation-based mass sensing using piezoelectrically-actuated microcantilevers. *Appl Phys Lett* 98(153510):1–3.
27. Craighead H (2007) Nanomechanical systems—measuring more than mass. *Nat Nanotechnol* 2:18–19.
28. Ramos D, Tamayo J, Mertens J, Calleja M, Zaballos A (2006) Origin of the response of nanomechanical resonators to bacteria adsorption. *J Appl Phys* 100(106105):1–3.
29. Gil-Santos E, et al. (2010) Nanomechanical mass sensing and stiffness spectrometry based on two-dimensional vibrations of resonant nanowires. *Nat Nanotechnol* 5:641–645.
30. Sadeghian F, Goosen H, Bossche A, van Keulen F (2010) Application of electrostatic pull-in instability on sensing adsorbate stiffness in nanomechanical resonators. *Thin Solid Films* 518:5018–5021.
31. Nair PR, Alam MA (2010) Theory of "selectivity" of label-free nanobiosensors: A geometro-physical perspective. *J Appl Phys* 107(064701):1–6.
32. Yang Y, Callegari C, Feng X, Ekinci K, Roukes M (2006) Zeptogram-scale nanomechanical mass sensing. *Nano Lett* 6:583–586.
33. Tilmans HAC, Legtenberg R (1994) Electrostatically driven vacuum-encapsulated polysilicon resonators part II. theory and performance. *Sensors Actuat A-Phys* 45:67–84.
34. Abelé N (2007) Design and fabrication of suspended-gate MOSFETs for MEMS resonator, switch and memory applications. PhD thesis (Ecole Polytechnique Federale De Lausanne, Lausanne, Switzerland).

Supporting Information

Jain et al. 10.1073/pnas.1203749109

SI Text

In this document we discuss the proof-of-concept of Flexure-FET biosensor and justify the various claims made in the paper using the experimental data available in the literature. Before we show the proof-of-concept, we want to mention that the operation of Flexure-FET consists of three main pieces: (*i*) stiffness change due to capture of biomolecules, (*ii*) operating the gate near pull-in instability for maximum change in the displacement, and (*iii*) subthreshold conduction of the FET for exponential sensitivity (Fig. S1). In the following sections we validate each of the three pieces and their combined actions.

Experimental Validation of Stiffness Increase Due to Capture of Biomolecules. The operating principle of the proposed Flexure-FET is based on the increase in the stiffness of a cantilever or fixed-fixed beam due to the capture of biomolecules. This increase in the stiffness due to capture of biomolecules has been reported by several groups (1–4). Fig. S2 shows one such dataset for percentage increase in the stiffness due to capture of proteins on different cantilevers (2). It should be noted that percentage increase could be as high as 50%. We have shown in the article that even a 5–10% increase in the stiffness results in two to three orders of magnitude change in the drain current.

Experimental Validation That Operation Close to Pull-In Instability Results in Maximum Change in the Displacement (Δy) Due to Change in the Stiffness (Δk). The second part of the operation of Flexure-FET; i.e., biasing the gate near pull-in maximizes Δy, has also been demonstrated in large numbers of experiments on electromechanical resonators (Figs. S3–S5) (5, 6). In the following, we interpret the experiments from the perspective of its application in Flexure-FET.

We recall that capture of biomolecules changes the stiffness $k \propto \frac{EWH^3}{L^3}$ due to change in the thickness H of the gate. Since $\frac{\Delta k}{k_0} = 3\frac{\Delta H}{H_0} + \frac{\Delta W}{W_0} + \frac{\Delta E}{E_0} - 3\frac{\Delta L}{L_0}$, where the subscript 0 indicates initial values, we note that the nonlinear sensitivity of Δy on Δk can be equivalently demonstrated by changing the beam length L (5) or Young's modulus E (6).

Fig. S4*A* shows the response of two electromechanical resonators (5) having different lengths. Their differential nonlinear response $\Delta y(V_G) \equiv y(k(L_1), V_G) - y(k(L_2), V_G)$ for two different lengths, $L_1 = 310$ μm and $L_2 = 510$ μm, is shown in Fig. S4*B*. Similarly, Fig. S5*A* shows the response of an electromechanical resonator (6) at two different temperatures. Nathanson, Newell, Wickstrom, and Davis (6) assume that an increase in temperature decreases the Young's modulus. The corresponding differential nonlinear response $\Delta y(V_G) \equiv y(k(T_1), V_G) - y(k(T_2), V_G)$ for two different temperatures (or different Young's modulus), $T_1 = 30\,^{\circ}\mathrm{C}$ and $T_2 = 80\,^{\circ}\mathrm{C}$, is shown in Fig. S5*B*. These experiments confirm that that any change in Δk is reflected in nonlinear response in Δy, and Δy is maximum close to pull-in instability—a key assertion of the Flexure-FET concept.

Experimental Validation That Drain Current in Flexure-FET Depends Exponentially on the Gate Position (y) in Subthreshold Regime. Fig. S6 shows the response of a suspended-gate FET (7). The structure of suspended-gate FET is similar to the proposed Flexure-FET, and therefore the experimental data is directly relevant. The symbols in Fig. S6*B* show the measured drain current as a function of gate voltage (7). Our numerical simulations (solid line in Fig. S6*B*) based on Eqs. **1** and **2** in the main text reproduce the experimental data very well. The drain current has been obtained using the following expression

$$I_{\mathrm{DS}} = \frac{qn_i^2}{N_A}\mu_n \frac{L}{W} V_{\mathrm{DS}} \int_0^{\psi_S} \frac{e^{\frac{q\psi}{mk_{\mathrm{B}}T}} - 1}{E_s(\psi)} d\psi, \qquad [\mathbf{S1}]$$

where the underlap factor $m \sim 5.5$ accounts for the fact that the membrane does not overlap the source/drain completely (8). Fig. S6*C* shows the drain current as a function of the position of the gate (y) confirming that drain current depends exponentially on y in subthreshold region. Therefore, any change in gate position will result in exponential change in the drain current.

Hence, all the three pieces of the Flexure-FET operation namely change in stiffness due to capture of biomolecules (Fig. S2), maximum change in gate position occurs close to pull-in due to change in stiffness (Figs. S4 and S5) and the exponential dependence of transistor drain current on the gate position in subthreshold (Fig. S6) are supported by experiments. In the following we conclude this discussion by showing the sensitivity of the devices discussed above when reconfigured in the Flexure-FET mode.

Response of Existing Devices When Reconfigured to Flexure-FET Mode. If the devices discussed above were reconfigured in the Flexure-FET mode, we anticipate the following response. If a transistor was integrated with the electromechanical resonators discussed in Figs. S4 and S5 and operated in the subthreshold regime, according to the theory discussed in the article, the overall response will be given by

$$\frac{I_{\mathrm{DS1}}}{I_{\mathrm{DS2}}} = \exp\left(\frac{(k_1/A_1)(y_0 - y_1) - (k_2/A_2)(y_0 - y_2)}{k_B T \epsilon_S N_A}\right), \qquad [\mathbf{S2}]$$

where $I_{\mathrm{DS1}}, k_1, y_1, A_1$ are initial drain current, stiffness, position, and area of the beam, whereas $I_{\mathrm{DS2}}, k_2, y_2, A_2$ are drain current, stiffness, position, and area due to stiffness change. In Eq. **S2** all the parameters are known experimentally except the doping of the substrate N_A. For a typical doping concentration ($N_A = 5e14 - 5e16\ \mathrm{cm}^{-3}$), the ratio of drain currents $\frac{I_{\mathrm{DS1}}}{I_{\mathrm{DS2}}}$ changes by two to three orders of magnitude, confirming the exponential sensitivity of this class of devices (Fig. S7 *A* and *B*). Similarly, if the membrane stiffness of suspended-gate FET was changed by approximately 30–35% (keeping all other parameters to be the same and underlap factor $m = 1$ in Eq. **S1**), a similar two to three order magnitude change in drain current is expected (Fig. S7*C*).

1. Craighead H (2007) Nanomechanical systems—Measuring more than mass. *Nat Nanotechnol* 2:18–19.
2. Gupta A, et al. (2006) Anomalous resonance in a nanomechanical biosensor. *Proc Nat Acad Sci USA* 103:13362–13367.
3. Ramos D, Tamayo J, Mertens J, Calleja M, Zaballos A (2006) Origin of the response of nanomechanical resonators to bacteria adsorption. *J App Phys* 100(106105):1–3.
4. Gil-Santos E, et al. (2010) Nanomechanical mass sensing and stiffness spectrometry based on two-dimensional vibrations of resonant nanowires. *Nat Nanotechnol* 5:641–645.
5. Tilmans HAC, Legtenberg R (1994) Electrostatically driven vacuum-encapsulated polysilicon resonators part II. Theory and performance. *Sensors and Actuators A Phys* 45:67–84.

6. Nathanson HC, Newell WE, Wickstrom RA, Davis JR, Jr. (1967) Resonant gate transistor. *IEEE Trans Electron Devices* 14:117–133.
7. Abelé N (2007) Design and Fabrication of Suspended-Gate MOSFETs for MEMS Resonator, Switch and Memory Applications. PhD thesis (Ecole Polytechnique Federale De Lausanne, Lausanne, Switzerland).
8. Paul B, Bansal A, Roy K (2006) Underlap DGMOS for digital-subthreshold operation. *IEEE Trans Electron Devices* 53:910–913.

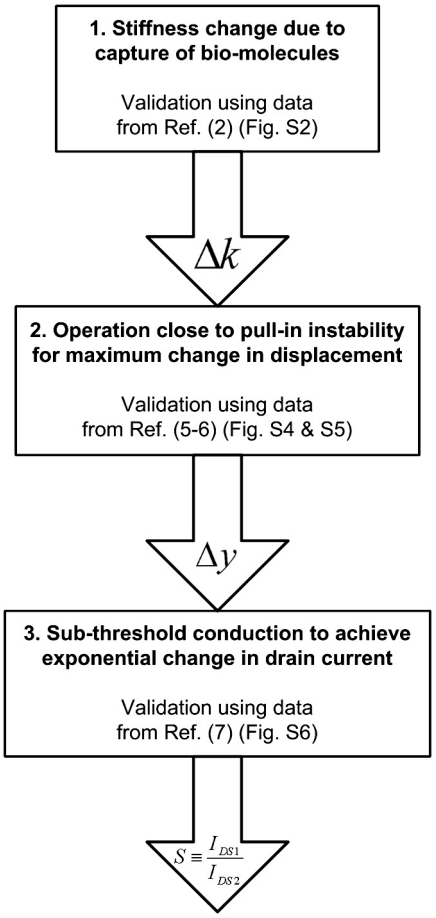

Fig. S1. Flow chart showing three main pieces of Flexure-FET operation for achieving exponential sensitivity. The flow chart also shows the references which are used to validate the various pieces.

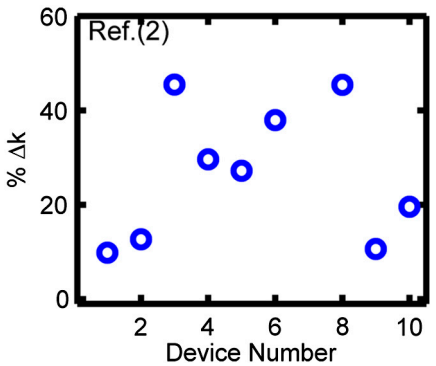

Fig. S2. Experimental validation of the first part (Part 1 in Fig. S1); i.e., change in stiffness due to capture of biomolecules on different nanocantilever devices (2).

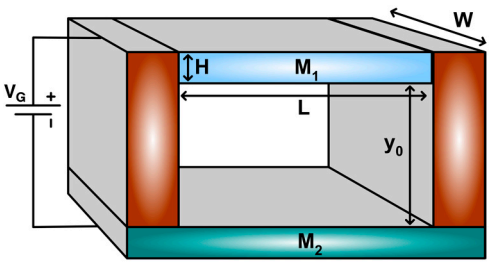

Fig. S3. Schematic of an electromechanical resonator.

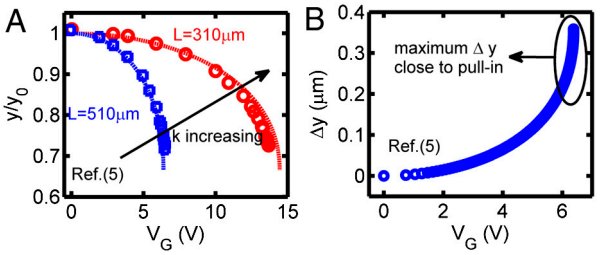

Fig. S4. Demonstration of nonlinear sensitivity of Δy on Δk using the response of two electromechanical resonators with different lengths (5). (*A*) Equilibrium position of beam as a function of applied bias. Symbols are the experimental data (5), and the dotted line is the numerical simulations based on Eqs. **1** and **2** in the article. Different symbols correspond to $L = 510$ μm (empty square) and $L = 310$ μm (empty circle). (*B*) Difference in the equilibrium position Δy as a function of gate voltage suggests that maximum change in Δy occurs close to pull-in instability.

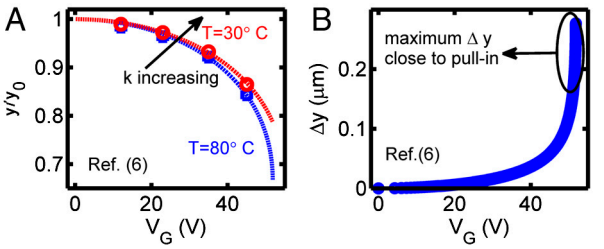

Fig. S5. Demonstration of nonlinear sensitivity of Δy on Δk using the response of an electromechanical resonator at two different temperatures (6). (*A*) Equilibrium position of the beam as a function of applied bias for two different temperatures 80 °C (empty square) and 30 °C (empty circle). Symbols are the experimental data, and the dotted line is the numerical simulations based on Eqs. **1** and **2** in the article. (*B*) Change in beam position Δy is due to change in temperature (and hence stiffness).

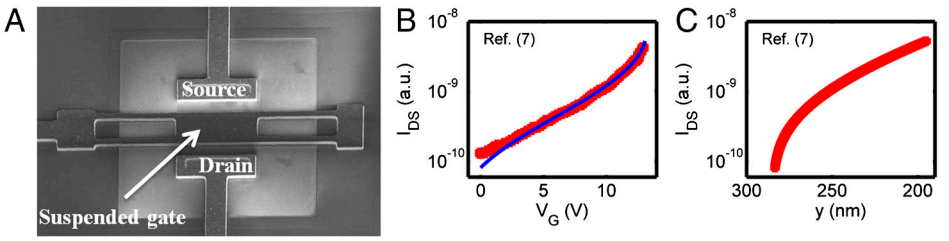

Fig. S6. Response of a suspended-gate FET (7). (*A*) Micrograph of the suspended-gate FET. (*B*) Measured drain current as a function of gate voltage. Symbols are the experimental data, and the solid line is the numerical simulation. (*C*) Corresponding drain current as a function of the position of gate (y) showing that drain current depends exponentially on y.

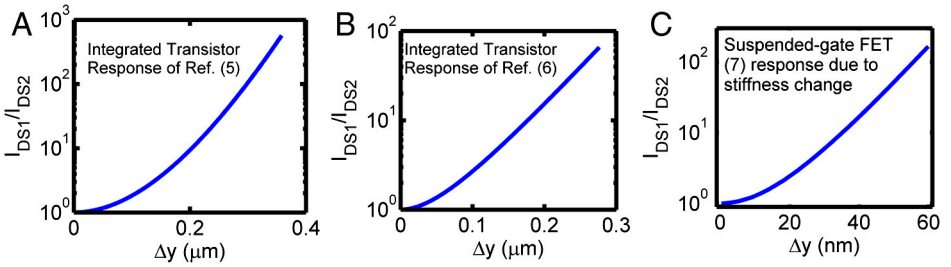

Fig. S7. Response of existing devices reconfigured to operate in Flexure-FET mode. (*A*, *B*) If a transistor is integrated with the existing electromechanical resonators (5, 6), drain current I_{DS1}/I_{DS2} changes by two to three orders of magnitude, as suggested in the article. (*C*) The response of suspended-gate FET (7) (with underlap factor $m = 1$) due to stiffness change ($\Delta k = 30$–35%) also suggests similar improvement.